Droplet polydispersity and shape fluctuations in AOT [bis(2-ethylhexyl)sulfosuccinate sodium salt] microemulsions studied by contrast variation small-angle neutron scattering

Lise Arleth and Jan Skov Pedersen*
Condensed Matter Physics and Chemistry Department, Risø National Laboratory, DK-4000 Roskilde, Denmark
(Received 20 June 2000; published 24 May 2001)

Microemulsions consisting of AOT water, and decane or iso-octane are studied in the region of the phase diagram where surfactant covered water droplets are formed. The polydispersity and shape fluctuations of the microemulsion droplets are determined and compared in the two different alkane types. Conductivity measurements show that there is a pronounced dependence of the temperature behavior of the microemulsion on the type of alkane used. In both cases the microemulsion droplets start to form larger aggregates when the temperature increases. But in the system with decane this aggregation temperature occurs at a temperature about 10 °C lower than in a similar system with iso-octane. Aggregation phenomena are avoided and the two systems are at approximately the same reduced temperature with respect to the aggregation temperature when the temperature of the AOT/D_2O/decane microemulsion is 10 °C and the temperature of the AOT/D_2O/iso-octane microemulsion is 20 °C. Contrast variation small-angle neutron scattering measurements are performed at these temperatures on systems with volume fractions of 5% D_2O+AOT by varying the scattering length density of the alkane. The small-angle scattering for 11 different contrasts evenly distributed around the match points are studied for each sample. The scattering data for the different contrasts are analyzed using a molecular constrained model for ellipsoidal droplets of water covered by AOT, interacting as polydisperse hard spheres. All contrasts are fitted simultaneously by taking the different contrast factors into account. The analysis show that at the same reduced temperature with respect to the aggregation temperature the droplet size, polydispersity index, the size of the shape fluctuations are similar in the two systems. A polydispersity index (σ/R of the Gaussian size distribution) of 16% and an average axis ratio of the droplets of 1.56 is found in the AOT/D_2O/decane microemulsion. In the AOT/D_2O/iso-octane system the polydispersity index is also 16% while the axis ratio is 1.72. The bending elastic constant κ and the Gaussian bending elastic constant $\bar{\kappa}$ can be estimated from these numbers. For AOT/D_2O/decane we find $\kappa=3.4k_BT$ and $\bar{\kappa}=-5.9k_BT$ and for AOT/D_2O/iso-octane we find $\kappa=2.35k_BT$ and $\bar{\kappa}=-3.8k_BT$, where k_B is the Boltzmann constant and T is the absolute temperature.

DOI: 10.1103/PhysRevE.63.061406 PACS number(s): 82.70.Kj, 61.12.Ex, 66.10.−x, 83.80.Hj

I. INTRODUCTION

Microemulsions are thermodynamically stable fluids composed of water and oil domains that are separated by a layer of surfactant molecules. The surfactants, which are molecules with a hydrophilic head and a hydrophobic tail, serve to stabilize the fluid and prevent it from macroscopic phase separation into water and oil. As the size of the water and oil domains is much smaller than the wavelength of visible light, the solutions appear optically isotropic and clear.

The microstructure of microemulsions varies a lot depending upon the actual system, composition, temperature, and additives. The simplest microemulsion systems are probably those composed of water, alkane, and nonionic surfactants of the type C_iE_j (alkyloligoglycolethers), where the C_i denotes an alkyl chain with i carbon atoms and the E_j denotes an ethylene oxide chain with j ethylene oxide groups. Taken at the right compositions and temperatures these systems form microemulsions. The system is an important model system and has therefore been studied very extensively over recent years by several groups (see, e.g., [1–3] and references therein). Both the chain length of the surfactant and the alkane type have been varied in these studies, which show that the system has some general features independent of the lengths of the surfactant and alkane. The behavior is conveniently summarized in the so-called fish-diagram [1]. When the phase behavior of the water/oil/C_iE_j system is plotted for equal volume fractions of water and oil and for varying surfactant concentration and temperature, a phase diagram that looks like the sketch of a fish is obtained (see Fig. 1). The system forms a microemulsion in the outer part of the fish tail. At low temperatures the microemulsion consists of oil droplets in water, at high temperatures the microemulsion consists of water droplets in oil, and in between the system forms a bicontinuous structure. In the head of the fish the system phase separates into a microemulsion phase and excess water and oil phases. At low temperatures (below the fish) the system phase separates into a microemulsion phase and an excess oil phase and at high temperatures (above the fish) the system separates into a microemulsion phase and an excess water phase. This temperature dependence of the system can be explained by the temperature dependent hydration of the surfactant's hydrophilic head group. At low temperatures the head group is very hydrated and takes up a relatively large space. This forces the film to be curved toward the oil side. As the temperature rises the head group becomes less hydrated and takes up less space and eventually the film becomes curved toward the water side.

The water/oil/C_iE_j system and its corresponding fish dia-

*Present address: Department of Chemistry, University of Aarhus, Lagelandsgade 140, DK-8000 Aarhus C, Denmark.

 ©2001 The American Physical Society

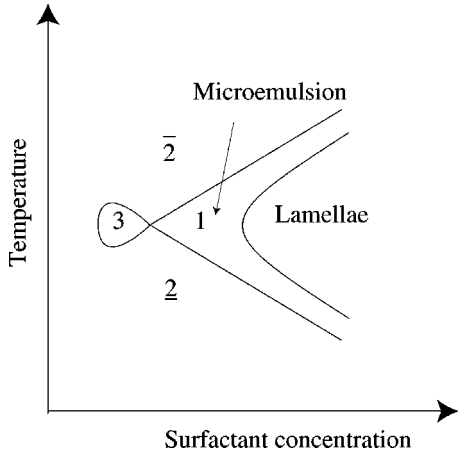

FIG. 1. The fish diagram. 1 denotes the one-phase microemulsion region. In the tail of the fish a lamellar phase is often present. $\underline{2}$ and $\overline{2}$ denote the two-phase regions. $\underline{2}$ consists of a microemulsion phase and an excess water phase and $\overline{2}$ consists of a microemulsion phase and an excess oil phase. 3 denotes the three-phase region. Here the sample separates into a microemulsion phase, an excess water phase, and an excess oil phase.

gram have served as a model both for polymer systems [4] and for systems composed of water, oil, and ionic surfactant, which we focus on in this article. It has been suggested that the phase behavior of microemulsion systems with ionic surfactants essentially resembles that of nonionic systems but with a reverse temperature dependence [5]. However, this comparison mainly holds in systems where the electrolyte effects of the ionic surfactants are partly screened by adding salt to the water [6]. In unscreened systems with ionic surfactants the situation is often less simple in practice. Even small impurities can have large effects on the phase behavior of the system [7,8] and uncritical use of the fish diagram with reverse temperature dependence as a sketch of the phase behavior of the system can be rather misleading.

The system we focus on in the present work is the bis(2-ethylhexyl)sulfosuccinate sodium salt (AOT)/water/alkane system. The volume fraction of the AOT/water droplets is approximately 5% and the system is studied in a part of the phase diagram where the microemulsion has the microstructure of AOT covered water droplets in oil. The aim is to get information about the polydispersity and shape fluctuations of the droplets by making a contrast variation small-angle neutron scattering (SANS) study of the fluids.

The study is inspired by the work of Rička, Borkovec, and Hofmeier from 1991 [9] and the work of Christ and Schurtenberger from 1994 [10]. Those authors demonstrate how the polydispersity of droplets in AOT/water/alkane microemulsions can be determined very precisely from contrast variation light scattering data in the vicinity of the optical match point. At zero angle the scattering depends, to first order, only on the volume distribution of the droplets and one therefore has a means of decoupling the polydispersity from the shape fluctuations. By these means Rička *et al.* obtained a polydispersity index of $\sigma/R_{av}=12\%$ in the AOT/water/hexane system, whereas Christ and Schurtenberger, surprisingly, obtained very different polydispersities in the AOT/water/iso-octane and the AOT/water/decane systems. In the case of decane, a number distribution with $\sigma/R_{av}=10\%$ was found and in the case of iso-octane $\sigma/R_{av}=19\%$ was found. σ is the standard deviation of the size distribution and R_{av} is the average radius.

Contrast variation light scattering exploits the fact that, since water and AOT have different dielectric constants, the optical contrast of the microemulsion droplets changes with the water to AOT ratio. The alkanes used for the study have dielectric constants that lie between those of water and AOT. It is therefore possible to combine water and AOT in such proportions that the average dielectric constant of water plus AOT is the same as that of the alkane used. At this point, which is normally referred to as the match point, a minimum in the forward scattering intensity is obtained. If all droplets in the microemulsion have exactly the same water to AOT ratio, the forward scattering will be zero at the match point. However, if the droplets are polydisperse they will have different water to AOT ratios and there is no single point where all droplets are matched out. Instead the forward scattering will show a minimum, which is also referred to as the match point. The more monodisperse the droplets are, the closer this minimum is to zero.

The work of Rička *et al.* and of Christ and Schurtenberger contributed to the ongoing discussion in the literature about the microstructure of microemulsions and the size of the polydispersity and shape fluctuations of microemulsion droplets. It has been predicted theoretically from a multiple chemical equilibrium approach [11,12] that the size polydispersity (σ_R/R) should be in the range 0.1–0.2. Experimentally, polydispersities in the range of 10% to 45% are found [2,13–18]. However, numbers between 15% and 25% are most often found. For the nonionic C_iE_j surfactants there is a dependence between polydispersity and surfactant type (length of alkyl chain) [2,19], whereas the polydispersity is independent of the alkane type [2].

Theoretical descriptions of the magnitude of the shape fluctuations are in general more vague since they depend on the value of the bending elastic constant κ and the Gaussian bending elastic constant $\bar{\kappa}$ [12,20,21]. Borkovec stated in 1992 that these numbers were not known very precisely [20]. At that time the numbers found for κ varied over an order of magnitude, between $0.5k_BT$ and $5k_BT$, where k_B is the Boltzmann constant and T is the absolute temperature. Since then much effort has been put into a more precise determination of the bending elastic constants and several techniques have been developed; however, as Gradzielski pointed out recently [22], the values determined for similar systems still vary significantly from one study to another. In interpretations of experiments the size of the shape fluctuations is often expressed in terms of the mean square amplitude $\langle|u_2|^2\rangle$ of $l=2$ terms of the spherical harmonics [2,14,15,21]. This corresponds roughly to the amplitude of peanutlike deformations. The parameter $\langle|u_2|^2\rangle$ is convenient for some purposes since it can be related to the bending elastic constant κ and the Gaussian bending elastic constant $\bar{\kappa}$ [20,21].

The aim of the present work is twofold: We want to investigate whether it is possible to obtain consistent and

unique information about both polydispersity and shape fluctuations of microemulsion droplets from small-angle scattering data and we want to determine the magnitude of the polydispersity and of the shape fluctuations.

It is well known that the small-angle scattering pattern from ellipsoids is equivalent to that of a distribution of polydisperse spheres. However, it has been shown by Caponetti *et al.* [23] that a distribution function leading to a scattering pattern equal to that of ellipsoids differs significantly from the distribution functions, that are normally expected for systems in thermodynamic equilibrium like microemulsions. The different distribution functions are clearly reflected in the high angular part of the scattering patterns. For spherical droplets distributed according to a Schulz or Gaussian distribution, the scattering pattern will lose the oscillations at high scattering angles as the polydispersity index increases. For monodisperse ellipsoidal droplets these oscillations remain to some extent. However, it is clear that it is very difficult to distinguish ellipsoids and polydisperse spheres from the high q part alone.

We therefore decided to use a similar strategy to that of Rička *et al.* and Christ and Schurtenberger but using small-angle neutron scattering instead of light scattering. We exploit the facts that SANS measurements provides information in a much wider interval of scattering vectors than light scattering measurements and that it is possible to make contrast variation by changing the scattering length density of the solvent by mixing protonated and deuterated solvent. In contrast to the light scattering measurements we can keep the water to AOT ratio and thereby the droplet size fixed. This seems at first sight to be a simpler method since we expect that a change from protonated to deuterated solvent will have a smaller effect on the samples than changing the droplet composition.

When we made our first set of SANS measurements on microemulsions of AOT/water/decane and AOT/water/iso-octane with droplet volume fractions at 5%, it was immediately evident that the two microemulsion systems have a significantly different behavior at room temperature. The data showed that the system with AOT/water/decane contains large aggregates of droplets at room temperature whereas the AOT/water/iso-octane system forms separated microemulsion droplets at room temperature. In order to get a better understanding of the systems, conductivity measurements were performed as a function of temperature on AOT/water/decane and AOT/water/iso-octane microemulsions with similar volume fractions of water and oil. The conductivity measurements suggested that the two systems would have similar microstructures with separated microemulsion droplets if the measurements on AOT/D_2O/decane were performed at 10 °C and the measurements on AOT/D_2O/iso-octane were performed at 20 °C.

The main points in the work described here are as follows. The contrast variation measurements were performed and the data at zero angle were analyzed in terms of a polydisperse hard-sphere model. Then the results of this analysis were compared to the data in the full q range. The agreement between this simple model and experiment was not satisfactory and the model had to be refined until we arrived at a model that on one hand was sufficiently detailed to account for all the details of the contrast variation data and on the other hand contained only the necessary number of fitting parameters. For the analysis the scattering data from all contrasts were analyzed simultaneously, using the same model for the full data set while taking the different contrast factors into account.

The final model consists of polydisperse prolate ellipsoids of revolution interacting as polydisperse hard spheres. At the end of the article we show that a description in terms of droplet polydispersity combined with the axis ratio gives estimates of the bending elastic constants κ and $\bar{\kappa}$.

II. EXPERIMENT

We used deuterated iso-octane and *n*-decane from Cambridge Laboratories. The decane has a purity of *d* of 99% and the iso-octane has a purity of *d* of 98%. The AOT was obtained from Fluka and has a purity of 99%. The D_2O was obtained from Aldrich Chemical Co. and has a purity of 99.9%.

All microemulsions were prepared by mixing the AOT, oil, and water in a vial. At room temperature the AOT dissolves easily in the alkane/water solutions. For reasons given in the following section, the contrast variation was performed by varying the ratio of protonated to deuterated alkane. The samples for the contrast variation measurements were prepared according to the following procedure. First stock solutions with volume fractions of 15% AOT and D_2O in, respectively, deuterated iso-octane and deuterated decane were prepared by weight. Both solutions had molar ratios of water to AOT (w_0) of 38. These two stock solutions were then diluted into four stock solutions by diluting half the 15 vol % solution of AOT and D_2O in alkane with hydrogenated alkane and diluting the other half with deuterated alkane. The final droplet volume fractions were 0.050 in the two AOT/D_2O/iso- octane solutions and 0.051 in the two AOT/D_2O/decane solutions. The two AOT/D_2O/iso-octane solutions were then mixed in different proportions in order to obtain varying degrees of protonation of the solvent and consequently varying scattering length densities. The same was done for the two AOT/D_2O/decane solutions. By preparing all samples from the 15 vol % stock solutions we were sure to keep w_0 constant within each of the two series of measurements. The molecular volumes, mass densities, and scattering length densities used for the calculations for the sample preparations as well as for the mathematical modeling of the microemulsion system are given in Table I.

The SANS measurements were performed at the SANS facility at Risø National Laboratory [24,25]. Using different combinations of neutron wavelengths and sample-to-detector distances, a q range from 0.004 $Å^{-1}$ to 0.26 $Å^{-1}$ was covered. A wavelength spread $\Delta\lambda/\lambda$ of 24% [full width at half maximum (FWHM)] as determined by the Bragg peaks from a silver behenate sample [26]. The wavelength spread was determined by making a SANS measurement on a silver behenate sample and fitting a Gaussian to the first order Bragg peak. The SANS data were azimuthally averaged and normalized by the standard approach by division by the scatter-

TABLE I. Molecular volumes (V), mass densities (ρ_m), and scattering length densities ρ_s of the microemulsion constituents.

	V (Å^3)	ρ_m (g/cm^3)	ρ_s (1/cm^2)
AOT	648	1.139	0.642×10^{10}
H_2O	30.0	0.998	-0.560×10^{10}
D_2O	30.0	1.109	6.385×10^{10}
h-iso-octane	274.1	0.692	-0.515×10^{10}
d-iso-octane	274.1	0.802	6.320×10^{10}
h-decane	323.6	0.732	-0.488×10^{10}
d-decane	323.6	0.845	6.588×10^{10}

ing spectrum of H_2O [27]. The instrumental resolution effects are taken into account in the data analysis by convolution with the appropriate resolution function at each setting [28]. This is done automatically by the programs used for data analysis

The fact that the contrast variation measurements were performed by changing the fractions of deuterated (*d*) and protonated (*h*) solvents made it in principle necessary to perform a background measurement of the solvent mixture for each contrast. As this would be both very time consuming and expensive in deuterated alkanes, we tried to make a shortcut by measuring only the backgrounds of pure *h*-alkane and pure *d*-alkane and then afterwards calculate the backgrounds of the mixed solvents by making linear combinations of the background spectra from the pure systems, as is often done for mixtures of H_2O and D_2O. However, this procedure does not work and the data at high scattering angles were clearly undersubtracted when the background was estimated in this way. It was therefore necessary to perform measurements of the background scattering from mixtures of *h*- and *d*-alkane. The measurements showed that for both decane and iso-octane mixtures, the relatively large size of the molecules result in an angular dependence of the scattering in the small-angle scattering domain as well as an excess of scattering for the mixtures compared to the backgrounds calculated as linear combinations (see [29] for a more thorough discussion of these effects). These scattering vector dependent backgrounds have been measured and subtracted in the experimental data shown in the present work.

The samples were contained in 1 mm Hellma quartz cells. For reasons given in the following section the measurements on the AOT/D_2O/decane solutions were performed at 10 °C whereas the measurements on the AOT/D_2O/iso-octane solutions were performed at 20 °C. For conductivity measurements, samples having equal volume fractions of water and oil were prepared. The samples had the same water to AOT ratio as the samples for the contrast variation measurements, i.e., $w_0=38$. A CDM80 conductivity meter from Radiometer, Copenhagen was used. Due to the high cost of the deuterated alkanes we made a conductivity cell that could be used for very small samples. The very simple cell is illustrated and explained in Fig. 2. With the dimensions we chose, it was possible to measure the conductivity of sample volumes down to 0.25 cm^3; however, it is also feasible to construct a smaller cell.

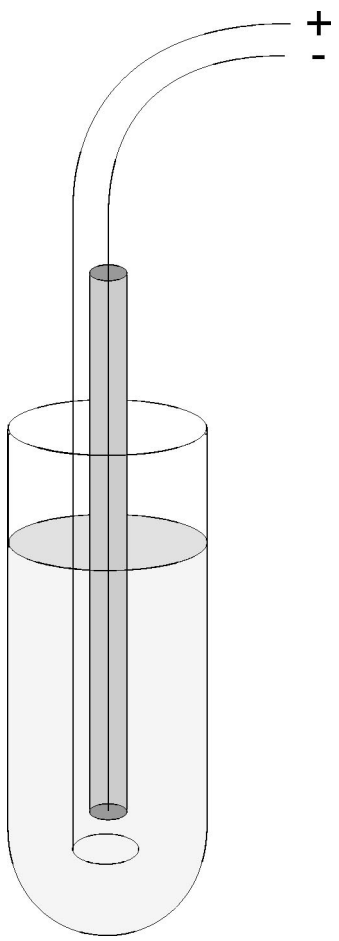

FIG. 2. The cell for conductivity measurements. For the anode a thin platinum wire has been melted into a glass tube. The cathode is a platinum wire that is bent into an O shape below the position of the anode. As the area of the anode is very small compared to the size of the cathode the cell constant is inversely proportional to the cross-sectional area of the anode.

III. CONDUCTIVITY MEASUREMENTS

As explained in the Introduction it is well known that the microstructure of microemulsions is strongly temperature dependent. It has been shown that a microemulsion with an ionic surfactant and equal volume fractions of oil and water with a little amount of salt added forms a microstructure with surfactant covered water droplets in a continuous oil phase (w/o) at low temperatures and surfactant covered oil droplets in continuous water phase (o/w) at high temperatures [1,5]. The temperature dependence of the microstructure is therefore the reverse of that of nonionic microemulsions. As for the nonionic microemulsions these changes in microstructure are driven by a change in the spontaneous curvature of the surfactant film with temperature [1]. Even though this picture may be too simplified for the AOT/water/alkane system, which differs from the above mentioned model system by both the lack of salt in the aqueous phase and by the impurities of the AOT [8], it is well known from several previous studies that the AOT/water/alkane system is very temperature dependent. At low temperatures a water-in-oil droplet structure is formed, whereas, when the temperature is in-

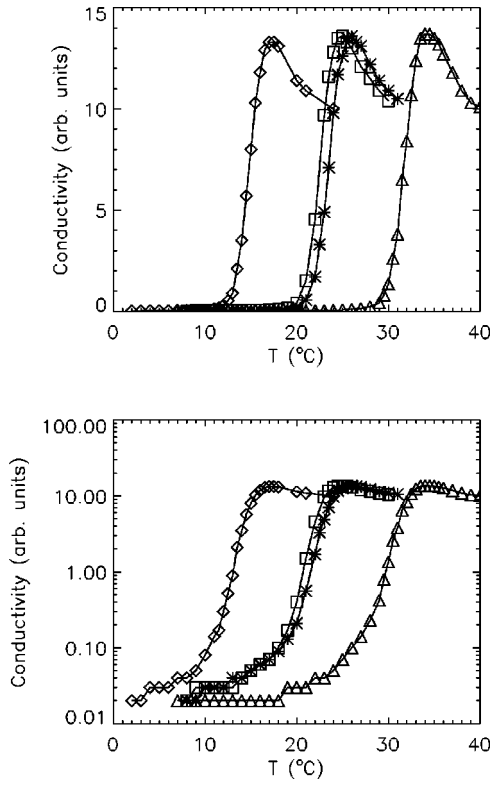

FIG. 3. The conductivity measurements of the four studied systems plotted on a linear (top) and a logarithmic (bottom) scale. ◇ is the AOT/H_2O/*h*-decane system, □ is the AOT/D_2O/*h*-decane system, * is the AOT/D_2O/*d*-decane system, and △ is the AOT/D_2O/*h*-iso-octane system.

creased, larger aggregates of droplets are formed [30–33].

A fast and easy way to determine the temperature at which the microstructure of an ionic microemulsion changes from a droplet structure to a structure with a continuous water phase is to measure the conductivity of the microemulsion as a function of temperature. At low temperatures where the microemulsion is continuous in the oil phase the conductivity will be very low. As the temperature is increased the droplets start to form clusters and eventually form larger networks that allow the counterions of the AOT to move around, causing an increase of the conductivity (see, e.g., [34–36]).

In order to study the effects that the change from protonated to deuterated solvents may have on the microstructure of the microemulsions, conductivity measurements were performed on solutions of AOT/H_2O/*h*-decane, AOT/D_2O/*h*-decane, and AOT/D_2O/*d*-decane. The conductivity of an AOT/D_2O/*h*-iso-octane emulsion as a function of temperature was also measured in order to study the effect of changing the alkane type.

The four series of measurements are shown in Fig. 3. A significant increase of the conductivity is observed within a fairly narrow temperature interval of approximately 6 °C. The very low conductivity observed before the onset of this temperature jump is characteristic for a w/o microstructure. The high conductivity observed at high temperatures is due to a structure with connected water domains as explained above.

TABLE II. Temperature intervals of the conductivity jumps for the four samples studied. $T_{off-set}$ is the temperature where the conductivity starts to increase and T_{max} is the temperature where the conductivity reaches its maximum.

Sample	$T_{off\text{-}set}$ (°C)	T_{max} (°C)
AOT/H_2O/*h*-dec	12	17
AOT/D_2O/*h*-dec	19	25
AOT/D_2O/*d*-dec	20	26
AOT/D_2O/*h*-iso	28	34

In all four series of measurements the conductivity reaches a maximum and then slowly starts to decrease again. We have not been able to find such an effect in the conductivity data in the literature. For the present study, we are mainly interested in the position of the transition from w/o microemulsions to microemulsions with connected water domains, and we have not investigated the effect further.

The temperature intervals where the conductivity jump occurs are given in Table II. Changing from decane to iso-octane shifts the temperature interval of the conductivity jump 9 °C upward in temperature. This observation is in good agreement with former measurements [34,36] and is connected to the decreasing penetration of solvent into the surfactant layer with increasing molecular weight of the solvent [36].

The measurements also show that changing from protonated to deuterated decane has little effect on the microemulsion, whereas changing from D_2O to H_2O shifts the conductivity jump 7 °C downward in temperature. The different masses of the hydrogen atoms in D_2O and H_2O have an effect on the hydrogen bonds between molecules, and the fact that the change from D_2O to H_2O causes a much larger change in temperature than the change from protonated to deuterated decane suggests that the water structure plays a very important role in the microemulsion phase behavior, whereas the actual mass densities of the different microemulsion constituents are less important.

In contrast variation small-angle scattering experiments one has to study the *same* structure at different contrasts in order to make a meaningful analysis. This is most often done by changing from protonated to deuterated solvent. However, as we have shown above such a change may influence the system so that instead of studying the same structures at different contrasts one ends up in a situation where different structures are studied at different contrasts. For the AOT/water/alkane system this solvent effect is much smaller if the contrast variation is performed by varying the degree of deuteration of the alkane than if that of water is varied.

IV. SCATTERING EXPERIMENTS

All contrast variation measurements are performed on microemulsions with low volume fractions of AOT + water (5.1% for the AOT/water/decane system and 5.0% for the AOT/water/iso-octane system). This very asymmetric com-

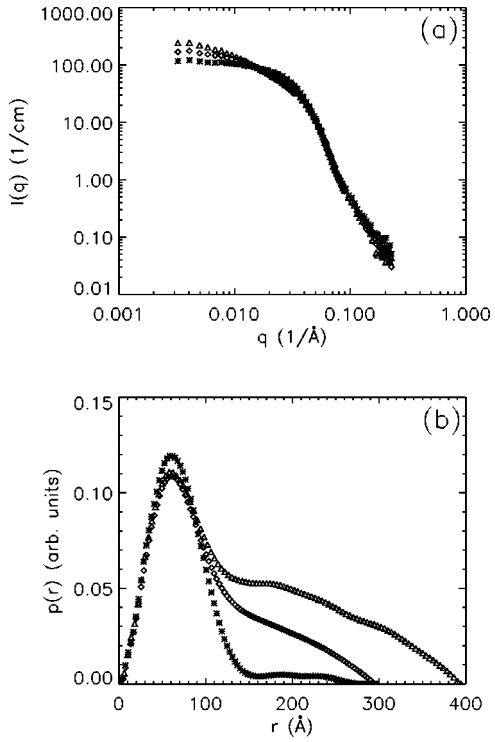

FIG. 4. Temperature dependence of AOT/D_2O/*h*-decane microemulsion (bulk contrast) with a volume fraction of 5%. (a) The scattering data and (b) the pair-distance distribution functions as obtained by indirect Fourier transform. * is taken at 15 °C, ◇ at 25 °C, and △ at 30 °C.

position of the microemulsion is of course most likely to enforce a w/o droplet structure in the full temperature range where the microemulsion is thermodynamically stable. However, the temperature dependence observed in the conductivity measurements for the symmetric microemulsions turns out to be reflected in the droplet interactions of these diluted systems. Figure 4(a) shows the scattering data obtained on a microemulsion with 5 vol % AOT and D_2O in *h*-decane for three different temperatures. The scattering at low angles increases with increasing temperature, which shows that the size of the droplets increases, probably due to the formation of clusters or aggregates of droplets. The effect is even more visible in the so-called pair-distance distribution functions, $p(r)$. The $p(r)$ function is related to the correlation function $\gamma(r)$ by $p(r)=r^2\gamma(r)$, and can be obtained by an indirect Fourier transformation [37] of the scattering data. As the name suggests $p(r)$ gives the distribution of distances within pairs of scattering centers in the droplets weighted by the scattering length densities of the points connected by the vector $\vec{r}$. For bulklike or homogeneous contrasts, like the one studied in Fig. 4, the value of r for which $p(r)$ goes to zero gives the maximum distance that occurs within the droplets. For the same contrast spherical objects give rise to a bell-shaped curve, and if the objects are elongated (or very polydisperse) $p(r)$ will have a tail and go to zero at a higher r value. This is exactly what we observe in Fig. 4(b), where the pair-distance distribution functions obtained by indirect Fourier transform are shown. We therefore interpret the temperature development of the $p(r)$ functions as being due to the formation of clusters or aggregates of droplets with increasing temperature. This interpretation is in agreement with earlier studies (see, e.g., [30,31]).

In order to safely avoid these aggregation phenomena we have performed the contrast variation measurements well below the onset of the conductivity jump in the symmetric microemulsions. Thus the measurements on the AOT/D_2O/decane solutions are performed at 10 °C whereas the measurements on the AOT/D_2O/iso-octane solutions are performed at 20 °C. The contrast variation measurements are performed by changing the ratio of *d*-alkane to *h*-alkane, and as the change from *d*-decane to *h*-decane has only a small effect in the conductivity measurements we expect the effect to be negligible in the contrast variation measurements.

The contrast variation measurements are shown in Fig. 5 (AOT/D_2O/decane) and Fig. 6 (AOT/D_2O/iso-octane). Each contrast is shifted by a factor of 5 in the plots. The scattering length densities of the solvents for the different contrast are written in the figures. In the lowermost data set in both figures the solvent is pure *d*-decane (*d*-iso-octane). This contrast is often referred to as the shell contrast, since the main contribution to the scattering comes from the AOT shell. In the uppermost data set in each of the figures the solvent is 2/3 *h*-alkane and 1/3 *d*-alkane. This contrast is a core-shell contrast with a positive excess scattering length density of the D_2O core and a negative excess scattering length density of the AOT shell. The match point, i.e., the point where the scattering length density of the droplets (water + AOT) on average is closest to the scattering length density of the solvent, is found between these two extrema, approximately at 1/3 *h*-alkane and 2/3 *d*-alkane. As we show in the following section the position of the match point is roughly determined by the degree of deuteration of the water core. In order to minimize the incoherent background as much as possible we generally wanted our system to have as high a degree of deuteration as possible. For this reason the match point was moved as much as possible to the deuterated side by using pure D_2O in the water cores.

V. ANALYSIS OF THE SANS DATA FOR THE MICROEMULSION SYSTEM

We assume that the microstructure of the microemulsion can be described as an isotropic suspension of droplets. The scattering from a system of polydisperse spherical objects is generally given by [38,39]

$$I(q)=\int_0^\infty dRN(R)f(q,R)^2+\int_0^\infty dRN(R)f(q,R)\times\int_0^\infty dR'N(R')f(q,R')H(q,R,R') \quad (1)$$

where $N(R)$ is the number size distribution function and $f(q,R)$ is the scattering form factor (amplitude) of a single spherical object of radius R and excess scattering length density $\rho(r)$. $H(q,R,R')$ describes the interparticle interferences between spheres with radii R and R'.

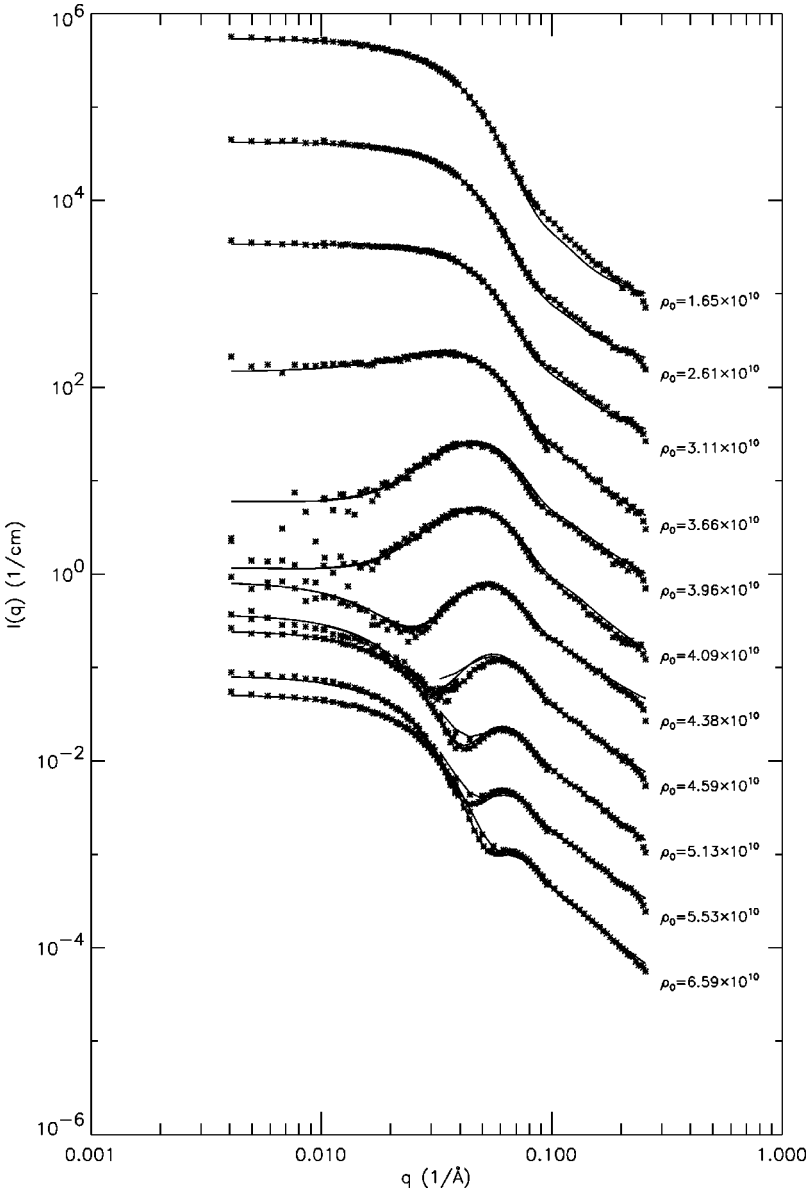

FIG. 5. Contrast variation SANS measurements on AOT/D_2O/decane. The full lines are the model fits. ρ_0 is in units of 1/cm^2. Each data set is multiplied by 5^n where n runs from -4 to 6 starting from the lowermost spectrum.

A. The distribution function

In the present work we have chosen $N(R)$ to be a Gaussian distribution in the droplet volumes. This choice of distribution function follows the results of the work of Eriksson and Ljunggren [11,12]. Using a multiple chemical equilibrium approach they predicted the distribution function, including the width of the size distribution for a given microemulsion. It turns out that the predicted distribution function is very similar to a Gaussian in the droplet volumes. For the fits we also tried to use a Gaussian number distribution and to use Schulz volume and number distributions, and in practice it did not make any significant difference.

A Gaussian volume distribution has the form

$$\phi(R) = Ce^{-(R-R_{av})^2/2\sigma^2} \tag{2}$$

so that the corresponding number distribution $N(R)$ becomes

$$N(R) = Ce^{-(R-R_{av})^2/2\sigma^2} \frac{1}{\frac{3}{4}\pi R^3}. \tag{3}$$

C is a normalization constant determined from the constraint

$$V_{droplet} = \int_{r_{min}}^{r_{max}} \phi(R) dR, \tag{4}$$

where $V_{droplet}$ denotes the volume fraction of the droplets (water cores) in the studied system and R is the droplet radius taken at the water-AOT interface.

For the fits $N(R)$ was calculated in the interval $r \in \{R_{av} - 4\sigma; R_{av} + 4\sigma\}$. However, if $R_{av} - 4\sigma < 0$, the distribution was cut off at zero. The distribution was approximated using 10 equidistant points.

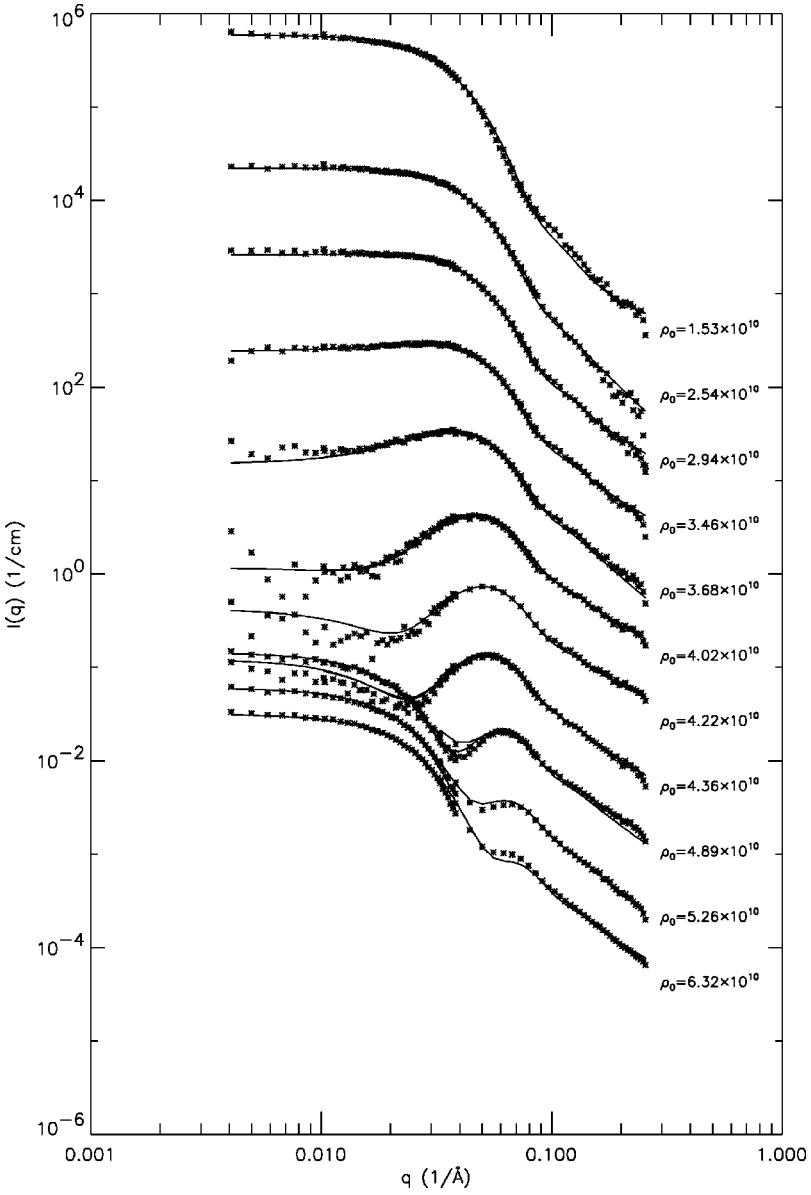

FIG. 6. Contrast variation SANS measurements on AOT/D_2O/iso-octane. The full lines are the model fits. ρ_0 is in units of 1/cm^2. Each data set is multiplied by 5^n where n runs from -4 to 6 starting from the lowermost spectrum.

B. The form factor

From the sample preparations we know the volume fractions of water and AOT in the microemulsions. This information is used as a constraint in the modeling and allows us to calculate the area per head group of the AOT molecules for a given size distribution of the droplets. For the calculation we have assumed that the area per head group of the AOT molecules taken at the water-AOT interface is constant for all droplet radii while the thickness of the AOT layer depends slightly on the radius. These constraints are included in the expressions given in the following.

The total surface area at the water-AOT interface per unit volume is calculated by integration over the droplet radius:

$$A=\int_{r_{min}}^{r_{max}} 4\pi R^2 N(R)dR, \tag{5}$$

where R is the radius taken at the water-AOT interface and $N(R)$ is normalized according to Eq. (4). The area per head group of the AOT molecules, A_{head}, is given by the fraction

$$A_{head}=A/N_{AOT}, \tag{6}$$

where the number of AOT molecules per unit volume, N_{AOT}, is given by V_{AOT}/v_{AOT}, where v_{AOT} is the molecular of the AOT molecule (see Table I).

Knowing A_{head} the dependence between the thickness of the AOT layer, D_{AOT}, and the core radius R is calculated from simple geometrical considerations. The number of AOT molecules, N_R, in a droplet of radius R equals $4\pi R^2/A_{head}$. The total volume of droplet and shell is $4\pi R^3/3+N_R\times v_{AOT}$; this volume is also equal to $4\pi(R+D_{AOT})^3/3$. Using this we get

$$D_{AOT}=\left(R^3+\frac{3R^2 v_{AOT}}{A_{head}}\right)^{1/3}-R. \tag{7}$$

From the sample preparations we also know the degree of deuteration of the alkane. Together with the information about the partial molecular volumes of the different constituents and their scattering lengths, this allows us to calculate the scattering length densities of the core and shell of the droplets and of the surrounding alkane.

We have used the scattering form factors of spheres [40] and ellipsoids [41] for the model calculations. The form factors are weighted by the volumes of the core and shell of the droplets and their scattering length densities. For a review of these form factors and many others, see [38].

For spherical droplets the form factor is

$$f(q)=V_c(\rho_c-\rho_s)F_1(qR_c)+(V_c+V_s)(\rho_s-\rho_0)F_1(qR_s), \tag{8}$$

where V_c and V_s are the volumes of core and shell, respectively, ρ_c, ρ_s, and ρ_0 are the scattering length densities of core, shell, and alkane, respectively, and R_c and R_s are the radii of core and shell, respectively. F_1 is given by [40]

$$F_1(qR)=3\frac{\sin(qR)-qR\cos(qR)}{(qR)^3}. \tag{9}$$

For the ellipsoidal droplets the form factor has to be orientationally averaged numerically:

$$\begin{aligned}\langle f(q)^2\rangle_o=\int_0^{\pi/2}&(V_c(\rho_c-\rho_s)F_1(qR_c\sqrt{\sin^2\theta+\varepsilon_c^2\cos^2\theta})\\&+(V_c+V_s)(\rho_s-\rho_0)F_1\\&\times(qR_s\sqrt{\sin^2\theta+\varepsilon_s^2\cos^2\theta})^2)^2\sin\theta d\theta.\end{aligned} \tag{10}$$

As above, V_c and V_s are the volumes of core and shell, respectively, ρ_c, ρ_s, and ρ_0 are the scattering length densities of core, shell, and alkane, respectively, R_c and R_s are the semiaxes of core and shell, respectively, and ε_c and ε_s are the axis ratios of core and shell, respectively.

For the fits the orientational averaging was performed over ten orientations evenly distributed between 0 and $\pi/2$. We have used the same volume distribution function for the ellipsoidal droplets as for the spheres, letting R in $\phi(R)$ denote the radius of a spherical droplet with the same volume as the ellipsoidal droplet.

The area per head group of the AOT molecules is calculated using an expression similar to Eq. (5) but with an expression for the surface area of, respectively, prolate and oblate ellipsoids [42]. If the droplet volume is kept constant the area per head group changes only slowly as the droplets are elongated or flattened into prolate or oblate ellipsoids. For example, for prolate ellipsoids with an axis ratio of 2, $A_l/A_{sph}\approx 1.024$, where A_l and A_{sph} are, respectively, the surface areas of an ellipsoid and a sphere with the same volume.

The thickness of the AOT layer of the ellipsoidal droplets is estimated using an expression similar to Eq. (7). By adding the D_{AOT} obtained to the minor and major axes of the water cores, we obtain ellipsoidal droplets covered with an AOT layer of approximately constant thickness. This leads to different axis ratios for the core and shell of the droplets, which it is straightforward to include in the form factor calculation [38].

C. The structure factor

About ten years ago Robertus *et al.* [13,30] made a small-angle x-ray scattering (SAXS) study of AOT droplets in a system of AOT/H_2O/iso-octane. The system was studied at temperatures between 25 ° and 37 °C where the microemulsion droplets become increasingly sticky and start to form clusters of droplets as the temperature rises. It was shown how the interactions between the sticky droplets as measured by SAXS could be modeled using the structure factor for polydisperse droplets interacting via a sticky hard-sphere potential. As described earlier we have deliberately chosen to perform our measurements at temperatures well below the temperatures where the droplets start to form clusters. Therefore, we did not use the model that includes stickiness of the spheres.

In the present work we have used the structure factor for a distribution of polydisperse hard spheres calculated in the Percus-Yevick approximation as given by Vrij [43–45]. This structure factor requires that the hard-sphere interaction radius R_{HS} for each droplet size and the hard-sphere volume fraction ν_{HS} are defined. We simply used $R_{HS}=R_S$ and $\nu_{HS}=\nu$, where R_S is the outer radius of the AOT shell and ν is the volume fraction of water plus AOT.

In principle this structure factor works only for polydisperse spheres but due to the lack of better models we also used it for the ellipsoidal droplets, substituting the $f(q,R)^2$ term of Eq. (1) with $\langle f_{ell}(q,R)^2\rangle_o$ and substituting the $f(q,R)$ term with $\langle f_{ell}(q,R)\rangle_o$, where $\langle\rangle_o$ denotes the orientational average. For the hard-sphere interaction radii of the ellipsoidal droplets we used the radii of spherical droplets of similar volume.

In the following we will make references to the effective structure factor $S_{eff}(q)$, which is

$$S_{eff}(q)=\frac{I(q)}{\int_0^\infty dRN(R)f(q,R)^2}, \tag{11}$$

where the numerator is given by expression (1) and the denominator is the pure form factor for scattering from the polydisperse droplets. It should be noted that $S_{eff}(q)$ depends significantly on the scattering length density profile of the droplets; this implies that the expression for $I(q)$ does not generally factorize into a product of a form factor and a structure factor even though this is often assumed. It should also be noted that for a droplet volume fraction of 5% the effective structure factor is still significant. If $R=60$ Å and the polydispersity index $\sigma/R=17\%$, then the effective structure factor $S_{eff}(0)\approx 0.7$ with a small dependence on the actual contrast. However, close to the match point $S_{eff}(q)$ is approaching unity and for monodisperse particles the structure factor effect vanishes totally at the match point. This can be understood by inspecting the second term of Eq. (1). The structure factor is weighted by the form factor. Since this

average is zero at the match point, the structure factor vanishes (see [46] for a more thorough discussion of the subject).

When analyzing contrast variation data measured around the match point, the fact that the structure factor vanishes at the match point has the important consequence that one cannot simply replace the structure factor by a constant at zero angle as was done by Gradzielski *et al.* [2]. If this is ignored, the depth of the minimum in $I(0)$ will be underestimated, leading to a too large value for the polydispersity index.

D. The scattering at zero angle

At zero angle the form factor expressions for both spherical and ellipsoidal droplets reduce to

$$f(0)=V_c(\rho_c-\rho_s)+(V_c+V_s)(\rho_s-\rho_0) \tag{12}$$

Inserting this expression in Eq. (1) and noting that to first order the structure factor is similar for spheres and ellipsoids at $q=0$, we see that the scattering at zero angle is a direct way of measuring the size distribution $N(R)$ of the droplets. In contrast there is no dependence on the shape of the droplets in the scattering at zero angle.

E. The fitting routine

We used a combination of the Levenberg-Marquardt method and a grid search for the model fitting [47]. Far away from the minimum the fitting parameters were optimized using the Levenberg-Marquardt method and close to the minimum the grid search was used. The error bars of the fitting parameters were estimated by changing one parameter a_i at a time and minimizing χ^2 by fitting the other parameters. The change δa_i that gives rise to an increase in χ^2 of $\chi^2/(N-P)$, where N is the number of data points and P is the number of fitting parameters, corresponds to the 68.3% confidence interval around a, i.e., to δa_i equal to the standard error [48]. This procedure takes into account correlations between the parameters.

VI. RESULTS AND DISCUSSION

The strategy of the data analysis we describe in the following is to extract the size distribution of the droplets first by analyzing the $I(0)$ data. Afterward the information about the shape of the droplets is obtained by analyzing the full q range. In this way we are in principle able to decouple the information about size and shape fluctuations in the scattering data. As explained in Sec. V the models used for the fits are all molecularly constrained and on an absolute scale.

A. The $I(0)$ data

Figure 7 shows model calculations of $I(0)$ for different sets of parameters. The sample composition is kept fixed at a volume fraction of 5% AOT + water and at a water-to-AOT ratio $w_0=38$. Model calculations for a system with pure D_2O cores are displayed in Fig. 7(a). The polydispersity index σ/R is varied, while the mean radius of the droplets is kept fixed at 60 Å. Increasing the polydispersity has a large

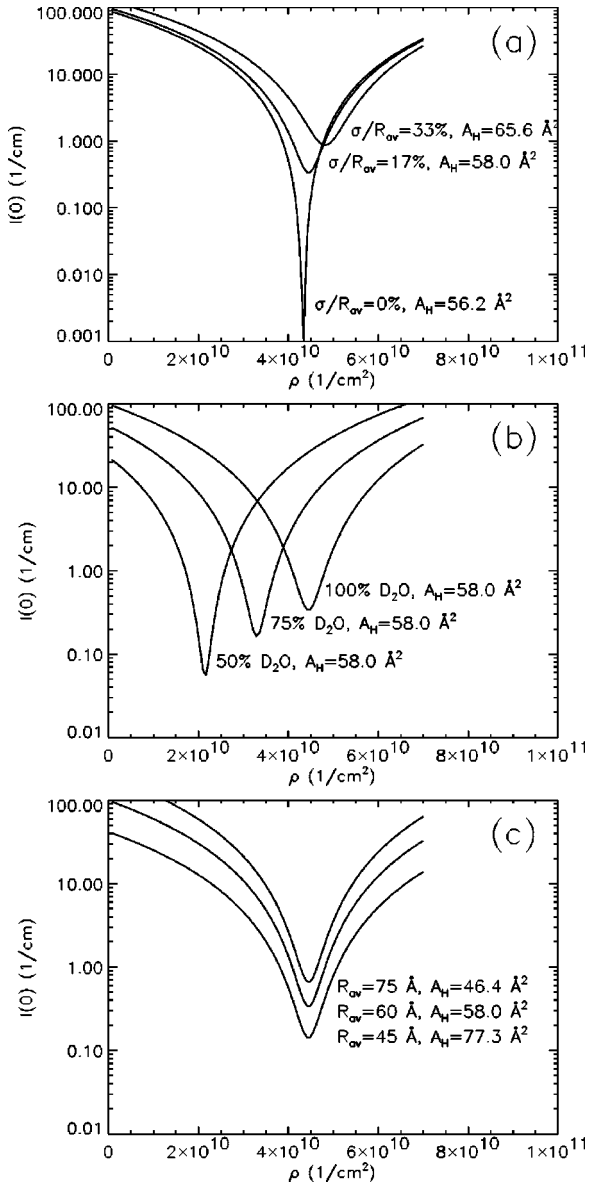

FIG. 7. The forward scattering for different model parameters. (a) The polydispersity is varied for a system with D_2O cores and with $R_{av}=60$ Å. The curves are for $\sigma/R_{av}=0$, 17, and 33 %. (b) The polydispersity is kept fixed at 17% and $R_{av}=60$ Å, and the scattering length of the water core is varied by varying the D_2O/H_2O fraction. (c) The droplet radius is varied for a system with D_2O cores and with $\sigma/R_{av}=17\%$. The curves are for $R_{av}=45$, 60, and 75 Å.

effect on the depth of the minimum in $I(0)$ at the match point. If the droplets are monodisperse, they will all have the same composition and the same average scattering length density of core and shell. Therefore, all droplets are matched out at the same scattering length density of the solvent, ρ_0. If the droplets are polydisperse, they also have different compositions and are consequently matched out at different scattering length densities of the solvent. We also note that the position of the match point moves slightly as the polydispersity index changes. The explanation for this is that the scattering intensity from the droplets is proportional to the vol-

ume of the droplets squared. This means that the large droplets scatter more than the small droplets and that the match point moves in the direction of the large droplets. Finally, we note that the area per head group, which is calculated by integration over the volume distributions, increases as the polydispersity index increases. The explanation for this is that the small droplets have a larger area per volume than the large droplets. When the polydispersity index increases, the volume fraction of the very small droplets and the total surface area of the solution increases. As the sample compositions are fixed in these calculations this implies that the area per head group increases.

In Fig. 7(b), the composition of the water core is varied while $R=60$ Å and $\sigma/R=17\%$ are kept fixed. The model is calculated for cores consisting of 50% H_2O/50% D_2O and 75% H_2O/25% D_2O, and finally for a core with 100% D_2O. As changing the composition of the water core leads to a change in the average scattering length density of the droplets, the main effect of this change is that the position of the match point is moved. However, we also note that the change has an effect on the absolute scattering length density at the match point. The reason for this is that the excess scattering length densities of water and AOT increase as the degree of deuteration of the water cores increases.

In Fig. 7(c), the model calculation is for a system with pure D_2O cores where the mean droplet radius is varied while the polydispersity index σ/R is fixed at 17%. This has an effect only on the absolute intensity of the scattering. As the calculations are performed for a fixed composition, the match point does not move. However, as the small droplets are more area consuming than the large droplets, the area per head group, calculated by integration over the volume distributions, increases.

To summarize we note that the depth of the minimum is mainly determined by the polydispersity index σ/R, the position of the minimum is mainly determined by the composition of the water cores (H_2O versus D_2O), and the absolute intensity is mainly determined by the mean radius of the droplets. For the fits we therefore took the mean radius, the polydispersity, and the purity of the D_2O as fitting parameters. When fitting the purity of the D_2O we assumed that the main impurity in the D_2O is H_2O. As it is well known that AOT comes with a small amount of water bound to it, a small contamination of H_2O is to be expected in the system. The water bound to the AOT and the water in the alkane will exchange with the D_2O of the water droplets, giving rise to a purity of the D_2O in the water cores lower than the 99.9% of the added D_2O.

The least-squares method used for the fitting procedure uses the statistical uncertainties σ_i as weights in the calculation of χ^2 [38]. These uncertainties are usually calculated from the counting statistics. This method of calculating the uncertainty implicitly assumes that the uncertainty on the ordinate of the points is vanishing, which makes sense in many experiments. However, in these contrast variation experiments the ordinate of the data points depends on the scattering length of the solvent, ρ_0, which again depends on the accuracy of the sample preparations.

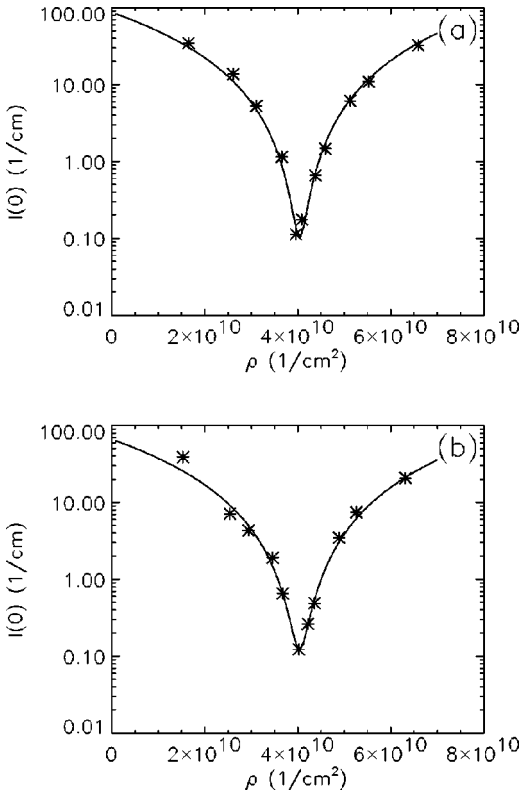

FIG. 8. The experimental data for $I(0)$ and the fitted model for (a) the AOT/D_2O/decane microemulsion and (b) the AOT/D_2O/iso-octane microemulsion.

We first tried to use the counting statistics uncertainties for the $I(0)$ data. But, due to the large difference in the absolute intensity between the points close to and the points far away from the match point, the points far away from the match point have relatively small uncertainties and therefore very large weight in the calculation of χ^2. In contrast, the points close to the match point, which are really the points that contain the information about the polydispersity, have almost no weight. So even though we obtained fits with relatively low χ^2, the agreement between experimental points and fits, when plotted on a logarithmic scale, was not satisfactory. We decided therefore simply to set the uncertainties of the experimental points to 10% of their values. In this way the points are evenly weighted in the fits, which makes sense as we expect the main uncertainty in the points to originate from the accuracy in the sample preparations.

The scattering data together with a least-squares fit of the model (12) are shown in Fig. 8. It shows the data for AOT/D_2O/decane [Fig. 8(a)] and AOT/D_2O/iso-octane [Fig. 8(b)]. The model parameters are given in Table III. The experimental data as well as the fits show that there are only minor differences in the droplet polydispersity in the two systems. The fits showed unexpectedly that the average radius of the droplets is larger in the AOT/D_2O/decane system than in the AOT/D_2O/iso-octane system.

The values determined for the polydispersity are comparable to the value determined by contrast variation light scattering by Rička, Borkovec, and Hofmeier, who found $\sigma/R_{av}=12\%$ in the AOT/water/hexane system [9] and to the

TABLE III. Parameters of the fits shown in Fig. 8. R_{av} denotes the mean radius of the water core of the droplets. σ/R_{av} denotes the polydispersity and Purity_{D_2O} is the purity of the D_2O. Note that A_{head}, the area per head group, is not a fitting parameter, but calculated by integration over the surface of the droplets in the model system.

Parameter	AOT/D_2O/dec	AOT/D_2O/iso
R_{av} (Å)	61.91±1.1	56.34±1.0
σ/R_{av}	0.094±0.009	0.120±0.010
Purity_{D_2O}	0.928±0.004	0.923±0.004
A_{head} (Å^2)	54.9±1.2	60.7±1.2

value of $\sigma/R_{av}=10\%$ determined by Christ and Schurtenberger [10] for the AOT/water/decane system. As mentioned in the Introduction, Christ and Schurtenberger measured very different polydispersities in the AOT/water/decane system and AOT/water/iso-octane system. Such a difference was not found in our experiments. A reason for the large difference in the polydispersities measured by Christ and Schurtenberger may be that the measurements on both systems were performed at 25 °C. At this temperature the droplets in the AOT/water/decane system will, according to our measurements, form larger aggregates, which has an effect on the $I(0)$ data.

It should be noted that polydispersities of 10%–12% are in the lower end of what is expected, both theoretically and experimentally, for the polydispersity of microemulsion droplets [2,11–18].

B. Analysis of the scattering data in the full q range

When we use the parameters obtained from the fit to the $I(0)$ data to calculate the scattering in the full q range, we get a good agreement between model and experimental data at low q values; however, at higher q values the modeled $I(q)$ is much more oscillatory than the experimental $I(q)$. This is shown in Fig. 9(a) for AOT/water/decane and in Fig. 9(b) for AOT/water/iso-octane. This suggests either that the droplets are more polydisperse than indicated by the $I(0)$ data or that they are nonspherical (or both).

As the $I(0)$ data, in principle, should contain the information about the volume polydispersity of the droplets, we first tried to fix the polydispersity at the value obtained from the $I(0)$ data. We then allowed the droplets to take the shape of ellipsoids of revolution by fitting the axis ratio of the droplets while keeping their volume and volume distribution fixed. This strategy, which seems very reasonable in theory, did not work in practice. Even though allowing the droplets to become ellipsoidal smears out the oscillations, the model curves were still much too oscillatory compared to the ex-

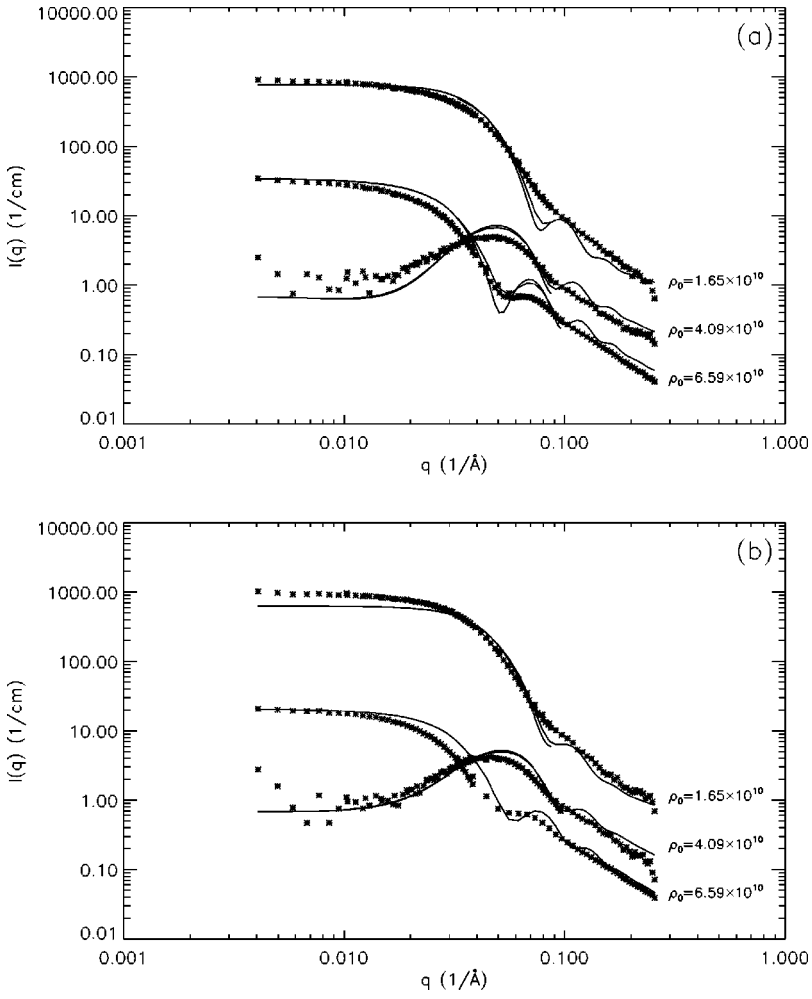

FIG. 9. The model fitted to the $I(0)$ data and experiment in the full q range. (a) The data from the AOT/D_2O/decane microemulsion taken for a shell contrast ($\rho_0=6.59\times10^{10}$ 1/cm^2), at the match point ($\rho_0=4.09\times10^{10}$ 1/cm^2), and for a bulklike contrast ($\rho_0=1.65\times10^{10}$ 1/cm^2). (b) Similar contrasts for an AOT/D_2O/iso-octane microemulsion. Each data set is multiplied by 5^n where n runs from 0 to 2 starting from the lowermost spectrum.

perimental curves. This suggests that the polydispersities determined from $I(0)$ data are too low.

In the next step we decided to disregard the information from the $I(0)$ data and fit a model for spherical droplets to the scattering data in the full q range. Introducing this modification of the model leads to reasonable fits and to an increase of the polydispersity index to 16% for both systems. The average droplet radius determined in this way is close to 60 Å for both systems. In the fits the hard-sphere volume fraction ν_{HS} was set equal to $c\nu$ where c is a fitting parameter and ν is the droplet volume fraction. In this way the effective hard-sphere structure factor is fitted. We expected c to be close to unity so that the effective hard-sphere volume fraction would be close to the droplet volume fraction, but the fits suggest that the hard-sphere volume fraction is close to zero, implying that the structure factor effects are almost vanishing. We believe that a possible explanation for this is that the fitting routine compensated for an incorrect form factor by lowering the importance of the structure factor. The next step was therefore to try to fit the model for ellipsoidal droplets again, but this time allowing the polydispersity to be different from the value determined from the $I(0)$ data. The fits obtained in this way were better and had a lower χ^2 than the fits with spherical droplets. However, the hard-sphere volume fraction ν_{HS} used for the structure factor calculation is still much lower than the droplet volume fraction.

For the first analysis the model fitted to the experimental data was relatively simple and contained only the average droplet radius R_{av}, the polydispersity index σ/R_{av}, the axis ratio of the droplets ϵ, the hard-sphere volume fraction divided by the droplet volume fraction c, and the purity of the D_2O together with an overall scale factor to take into account errors in the absolute scale. Backgrounds for the different spectra were also fitted in order to account for minor errors in the subtraction of the incoherent backgrounds.

During the process of data analysis we tried to improve this basic model in several different ways which are listed, explained, and discussed below.

Separation of the AOT shell into a polar and an apolar layer

The AOT molecule can be separated into a hydrophobic tail consisting of the two 2-ethylhexyl chains and a hydrophilic head group consisting of the rest of the molecule [49]. This means that the tail is composed of 16 C and 34 H, while the head group is composed of 7 O, 4 C, 3 H, 1 Na, and 1 S. If it is assumed that the 2-ethylhexyl chain has the same density as 3-ethylhexane (0.714 g/cm^3), the molecular volume of the hydrophobic chains is 526 Å^3 and the molecular volume of the head group is 122 Å^3. The scattering lengths of the hydrophobic and hydrophilic parts are then, respectively, -0.395×10^{10} 1/cm^2 and 5.12×10^{10} 1/cm^2. The separation of the AOT shell into a polar and an apolar layer improved the quality of the fits without changing any of the conclusions significantly.

Water molecules bound in the AOT shell

When the AOT is dissolved in water, water molecules will form hydrogen bonds to the polar part of the AOT molecule. For this reason the model was modified to allow for some of the water molecules to enter the AOT shell. We fitted a parameter n_H, which is the number of water molecules per AOT molecule in the hydrophilic shell. But as n_H quickly converged to a value near zero we concluded that the value of n_H is too low to be visible in the experiment and decided to fix n_H to zero.

Surface roughness of the AOT layer

A roughness of the AOT/alkane interface was implemented by multiplying the form factor by $\exp[-(qS_R)^2/2]$, where S_R is the surface roughness [50]. This modification improved the quality of the fits at high q values.

Layer of densely packed water near the AOT interface

It was previously shown by Svergun [51] by SAXS measurements on solutions of proteins that a thin layer of densely packed water is present at the protein-water interface. We placed a thin layer of densely packed water inside the droplets next to the the AOT film. The thickness of this layer was fixed at 2.6 Å and the scattering length density of the layer was set to $X_{\rho_{D_2O}}\times\rho_{D_2O}$ where $X_{\rho_{D_2O}}$ is a fitting parameter. In the fits $X_{\rho_{D_2O}}\approx1.25$. The numbers for $X_{\rho_{D_2O}}$ and the used thickness of the hydration layer are in good agreement with the numbers determined by Svergun [51] and the modification improved the quality of the fits.

Small AOT micelles in the alkane

This modification is suggested by the work of North *et al.* [52] and Svergun *et al.* [53]. Both groups analyzed series of small-angle x-ray scattering data on AOT microemulsions and concluded that some of the AOT forms small ''dry'' micelles in the alkane solution. Our model was modified to allow for such small micelles in the alkane and the volume fraction of AOT present in small micelles was fitted. As the volume fraction of the small micelles quickly converged to a value near zero we decided not to include this effect in the model.

Errors of the sample preparations

As explained in the experimental section the samples for the different contrasts were prepared by mixing two stock solutions in different proportions by weight. As very small amounts of sample were prepared, approximately 0.25 cm^3 for each contrast, small errors can have relatively large importance for the scattering length of the solvent. The $I(0)$ data points should in theory fall on a parabola, but as observed in Fig. 8 some of the data points are off this parabola. The main reason for this is the uncertainty of the scattering length of the solvent originating from the accuracy of the sample preparations. Therefore we decided to implement the possibility of accounting for imprecise sample preparations in the model. This was done in practice by allowing a small volume fraction of the *d*-alkane to be *h*-alkane (or the opposite) and fitting this uncertainty for each of the contrasts. The fitted uncertainties are generally very small (less than 2%)

TABLE IV. Parameters of the fits shown in Figs. 5 and 6. R_{av} is the mean radius of the water core of the droplets. σ/R_{av} is the polydispersity, ϵ is the axis ratio of the water cores, c is the hard-sphere volume fraction divided by the droplet volume fraction, S_R is the surface roughness, and Purity_{D_2O} is the purity of the D_2O. Scale is a constant overall scale factor. Note that A_{head}, the area per head group, is not a fitting parameter, but calculated by integration over the surface of the droplets in the model system. χ^2 is a measure of the deviation between experimental data and model.

Parameter	AOT/D_2O/dec	AOT/D_2O/iso
R_{av} (Å)	60.74±0.11	61.81±0.11
σ/R_{av}	0.1567±0.0004	0.1564±0.0008
ϵ	1.558±0.017	1.716±0.017
c	0.251±0.053	0.684±0.020
S_R(Å)	2.89±0.05	2.24±0.04
Purity_{D_2O}	0.9281±0.0005	0.9308±0.0005
Scale	0.8980±0.0018	0.7804±0.0014
$X_{\rho_{D_2O}}$	1.276±0.006	1.227±0.005
A_{head} (Å^2)	54.22±0.15	53.11±0.15
χ^2	6.25	5.62

and randomly distributed around zero. The modification improved the quality of the fits significantly without changing any of the conclusions.

We tried fitting a model for polydisperse hard sphere as well as a model for polydisperse hard ellipsoids with the modifications listed above. Again, the best fits (i.e., the lowest χ^2) were obtained with the model for ellipsoidal droplets. The fits are shown in Fig. 5 (AOT/water/decane) and Fig. 6 (AOT/water/iso-octane) and the fitting parameters are listed in Table IV. It should be noted that, even though the fits were improved significantly by the modifications listed above, the main parameters of the fits, R_{av}, σ, ϵ, and the purity of D_2O, were essentially unchanged.

Table IV shows that the model parameters are very similar in the two microemulsion systems. For AOT/water/decane the average radius is 60.7 Å, the polydispersity index is 0.16, and the axis ratio is 1.56. For AOT/water/iso-octane values of 61.8 Å, 0.16, and 1.72 are determined. This results in areas per head group that are also very similar in the two systems, 54.2 Å^2 for AOT/water/decane and 53.1 Å^2 for AOT/water/iso-octane.

The similarity of the results for the iso-octane and decane systems disagrees with the results of the analysis of the $I(0)$ data, which suggest that the droplets in AOT/water/decane and AOT/water/iso-octane have different values for the droplet radius, polydispersity index, and area per head group. Since many more data points containing much more information are fitted in the analysis of the data in the full q range, this latter analysis is much more reliable. However, it should be noted that the values for the purity of the D_2O as determined from $I(0)$ data and $I(q)$ data are very close, which they should be, as the modeled position of the match point is mainly determined by this parameter in both approaches. Values of 0.92–0.93 may seem low for the purity of the D_2O, but it should be remembered that this is not the purity of the D_2O as provided by the manufacturer, but the purity of D_2O in the water cores, where both Na^+ counterions from the AOT and H_2O molecules bound to the AOT are present. The different results of the analysis of the $I(0)$ data and the $I(q)$ data will be discussed further in Sec. VI C.

The effective hard-sphere volume fractions used for the structure factor calculations are in both cases significantly smaller than the droplet volume fractions. In the system with AOT/water/decane the effective hard-sphere volume fraction is as low as $\nu_{HS}\times 0.25$, where $\nu_{HS}=0.051$. This means that the structure factor effects almost vanish. This is surprising and suggests that the droplets are still somewhat sticky [13,31] at these low reduced temperatures. These effects cannot be modeled directly by the hard-sphere structure factor we are using, but in both approaches the model would compensate for the effects by lowering the hard-sphere volume fraction.

It has also been necessary to fit overall scale factors for the models. This is mainly done in order to compensate for errors on the absolute scale of the data. Usually values of unity within about 10% are to be expected. As all scattering data are converted to an absolute scale using the same H_2O spectrum, the scale factors should be identical for the two systems. But as seen in Table IV the scale factor fitted for the AOT/water/iso-octane data is lower than the scale factor fitted for the AOT/water/decane system. This is probably the result of some apparent systematic errors in the absolute scale of the iso-octane data which are reflected very clearly in the $I(0)$ data from the iso-octane system. As mentioned earlier these data should form a parabola, but as seen in Fig. 8(b) some of the points fall relatively far from the parabola, especially at low values for the scattering length density. The fitting routine compensates for these errors by adjusting the scale factor.

We have not listed the uncertainties of the sample preparations, which are also fitted in the routine. The values obtained for the uncertainties correspond to an uncertainty of less than 2% of the values for the fractions of deuterated and protonated alkane obtained by weighing during the sample preparations. A higher precision cannot be expected for the very small amounts of sample prepared for the experiments. However, for two of the samples higher numbers for the uncertainty were obtained (up to 6%). These were the AOT/water/iso-octane samples corresponding to the two leftmost points in Fig. 8(b), which fall far away from the parabola in the $I(0)$ curve as mentioned above. Uncertainties in the sample preparations of this magnitude are unrealistic. Disregarding these two contrasts from the iso-octane data the fitted uncertainties are generally randomly distributed around zero. It is important to note that the determination of the uncertainties was one of the last steps in the fitting procedure. This combined with the small and randomly distributed uncertainties ensures that fitting the uncertainties filters away small systematic errors in the contrast factors rather than forcing the data to fit the model, which one needs to be aware of.

The actual numbers for R_{av} and σ/R_{av} depend slightly on the type of distribution function used. As explained earlier we have used a Gaussian volume distribution in the present work. The numbers for the radius and the polydispersity ex-

pressed in terms of a Gaussian number distribution [denoted $N(R)$] are $R_{av,N(R)} \approx 54$ Å for $R_{av,\phi(R)} = 61$ Å, and $\sigma/R_{av,N(R)} \approx 0.17$ for $\sigma/R_{av,\phi(R)} = 0.16$. If the Schulz distribution is used the polydispersity is given in terms of the parameter z. The relation between σ/R_{av} and z is given by $\sigma/R_{av} = 1/\sqrt{z+1}$. This means that $\sigma/R_{av,\phi(R)} = 0.16$ corresponds to $z \approx 38$ for the Schulz volume distribution and $z \approx 35$ for the corresponding Schulz number distribution.

C. Comparison of measurements of polydispersity determined from $I(0)$ data and from $I(q)$ data

It is interesting to note that the polydispersities determined from $I(0)$ data are significantly lower than the polydispersities determined from the $I(q)$ data (compare Tables III and IV). As explained previously, the $I(0)$ data are analyzed using a form factor for polydisperse spherical droplets together with a polydisperse hard-sphere structure factor. Since only the volume distribution of the droplets is visible in the $I(0)$ data, it is reasonable to assume a form factor for polydisperse spherical droplets instead of a form factor for ellipsoidal droplets. However, Monte Carlo simulations [54] have shown that nonsphericity of the microemulsion droplets generally leads to increased importance of the structure factor at low angles. This effect grows as the axis ratio of the droplets becomes larger and it is obviously more visible in the $I(0)$ data than in the $I(q)$ data where the structure factor plays a role only for small q-values. To our knowledge, no closed expressions exist at present for the structure factor for polydisperse ellipsoidal droplets and from the above mentioned Monte Carlo simulations it is unfortunately not possible to predict how $S_{eff}(0)$ will be modified close to the match point with increasing axis ratio.

From our measurements it looks as if the nonsphericity of the droplets results in a depression of $I(0)$ near the match point, leading to a too low value for the polydispersity. This could be the result of an underestimate of $S_{eff}(0)$ near the match point. A similar tendency can be observed in the measurements by Christ and Schurtenberger [10] where a polydispersity index of 19% is found in the AOT/water/iso-octane system and 10% is found in the AOT/water/decane system. As explained earlier the measurements by Christ and Schurtenberger are performed at a temperature where large aggregates are present in the AOT/water/decane system. These aggregates will definitely be very anisotropic, which might result in an apparent value for the polydispersity that is too low, similarly to what we observe. The reason that the lowering of the $I(0)$ was not observed by Christ and Schurtenberger in the AOT/water/iso-octane system is probably that the droplet volume fractions are very low in their measurements so that the structure factor comes into play only when the droplets become very anisotropic. However, in order to test this theory, it is necessary to investigate the dependence between the contrast situation and axis ratio of the droplets further. This can be done either by determining a closed expression for the structure factor of polydisperse ellipsoidal droplets or by performing Monte Carlo simulations.

D. Determination of the bending elastic constant κ and the Gaussian bending elastic constant $\bar{\kappa}$

As mentioned in the Introduction the size of the shape fluctuations is often expressed in terms of the average amplitude $\langle |u_2|^2 \rangle$ of $l=2$ oscillations of the spherical harmonics. The angular dependent radius of the modeled droplet in terms of the spherical harmonics $Y_{lm}(\phi,\theta)$ is expressed as [56]

$$R(\theta,\phi) = R_{av}\left(1 + \sum_{l,m,l\neq 1} u_{lm} Y_{lm}(\theta,\phi)\right). \tag{13}$$

The polydispersity is given by the $u_{00}Y_{00}(\theta,\phi)$ term and the shape fluctuations are to first order given by the $u_{2m}Y_{2m}(\theta,\phi)$ term. Due to the averaging over orientation and size in both experiment and model it is in practice possible to determine only the mean-squared amplitudes $\langle |u_0|^2 \rangle$ and $\langle |u_2|^2 \rangle$, where $\langle |u_2|^2 \rangle$ is averaged over the five u_{2m}'s. The exact shape is therefore not given as it is a result of the individual u_{2m}'s. This is discussed further by Milner and Safran in [55]. They estimate the bending energy of the droplet shapes as a function of the values of the u_{2m}'s and conclude that the minimal energy shape is that of prolate ellipsoids of revolution, which is obtained when one of the u_{2m}'s is nonzero and the rest of the u_{2m}'s are equal to zero.

If we choose the solution $|u_{20}|^2 = c$ and $|u_{2m}|^2_{m\neq 0} = 0$, the average droplet shape is given by

$$\begin{aligned} R(\theta,\phi) &= R_{av}(1 + \sqrt{\langle |u_{00}|^2 \rangle} Y_{00}(\theta,\phi) + \sqrt{\langle |u_{20}|^2 \rangle} Y_{20}(\theta,\phi)) \\ &= R_{av}\Bigg(1 + \sqrt{\langle |u_{00}|^2 \rangle}\,\frac{1}{2\pi} \\ &\quad + \sqrt{\langle |u_{20}|^2 \rangle}\,\frac{5}{4}\sqrt{\frac{5}{\pi}}[3\cos^2(\theta) - 1]\Bigg). \end{aligned} \tag{14}$$

This average droplet shape is very close to the shape of a prolate ellipsoid with a droplet polydispersity of approximately

$$\sigma/R_{av} = \sqrt{\frac{\langle |u_{00}|^2 \rangle}{4\pi}}, \tag{15}$$

where the contributions from entropy of mixing and the higher order spherical harmonics are ignored [2,56].

An estimate of the average axis ratio ϵ of the average droplet shape is easily calculated as

$$\epsilon = \frac{R(0)}{R(\pi/2)} = \frac{1 + u_{00}/2\sqrt{\pi} + \frac{10}{4}\sqrt{5/\pi}u_{20}}{1 + u_{00}/2\sqrt{\pi} - \frac{5}{4}\sqrt{5/\pi}u_{20}} \tag{16}$$

where we have used the notation $u_{l0} = \sqrt{\langle |u_{l0}|^2 \rangle}$. The relations (15) and (16) can be used to convert the polydispersity index σ/R_{av} and axis ratio ϵ into the amplitudes $\langle |u_{00}|^2 \rangle$ and $\langle |u_{20}|^2 \rangle$ or vice versa. This makes it possible to make a direct comparison between the parameters obtained using the different types of models.

TABLE V. The parameters determining the shape fluctuations and polydispersity from different measurements. σ/R_{av} is the polydispersity, ϵ is the axis ratio, $\langle|u_{00}|^2\rangle$ and $\langle|u_{20}|^2\rangle$ are the mean-squared amplitudes of, respectively, the $l=0$ and $l=2$ oscillations of the spherical harmonics. κ is the bending elastic constant and $\bar{\kappa}$ is the Gaussian bending elastic constant. The numbers marked by an asterisk are the numbers stated by the authors. The remaining numbers are derived in the present work from these values. The numbers written in parentheses are the values derived by the authors. The error bars on κ and $\bar{\kappa}$ determined for AOT/D_2O/decane and AOT/D_2O/iso-octane are deduced from the error bars on σ/R_{av} and ϵ given in Table IV.

σ/R_{av}	ϵ	$\langle\|u_{00}\|^2\rangle$	$\langle\|u_{20}\|^2\rangle$	κ (k_bT)	$\bar{\kappa}$ (k_bT)	System
0.157*	1.56*	0.310	0.0133	3.4 ± 0.2	-5.9 ± 0.4	Present measurements
0.156*	1.72*	0.306	0.0201	2.35 ± 0.1	-3.8 ± 0.2	AOT/D_2O/decane AOT/D_2O/iso-octane
0.22*	1.47	0.61	0.011*	3.9 (3.8)	-7.2 (-7.5)	AOT/D_2O/decane [14]
0.17 (0.20)	2.5	0.34	0.062	0.92*	-0.38*	$C_{10}E_5$/D_2O/octane [57]
0.17 (0.15)	2.2	0.29	0.043	1.25*	-0.80*	$C_{10}E_5$/D_2O/*n*-dodecane [15]

Using the formalism of Safran [21] it is furthermore possible to convert the values for $\langle|u_{00}|^2\rangle$ and $\langle|u_{20}|^2\rangle$ into estimates of the bending elastic constant κ and the Gaussian bending elastic constant $\bar{\kappa}$ of the surfactant film by solving the following equations with respect to κ and $\bar{\kappa}$:

$$\langle|u_{00}|^2\rangle=\frac{k_BT}{12\kappa-8(R/R_0)(\kappa+\bar{\kappa}/2)+6\bar{\kappa}} \tag{17}$$

and

$$\langle|u_{20}|^2\rangle=\frac{k_BT}{16(R/R_0)(\kappa+\bar{\kappa}/2)-12\bar{\kappa}}, \tag{18}$$

where R_0 is the droplet radius at the emulsification boundary.

In Table V the values we have obtained for the polydispersity and shape fluctuations are listed and compared to values obtained by other groups. Different groups use different approaches to obtain these values. In [14] a combination of SANS and neutron spin echo (NSE) is used. In [15] and [57] a combination of SANS, NSE, and dynamic light scattering is used. The numbers marked by an asterisk are the numbers stated by the authors in their respective papers; the remaining numbers are derived using the relations given above. The numbers written in parentheses were derived by the authors in their respective papers. As seen these numbers differ slightly from the numbers derived using the equations above, which is because the above equations (15)–(18) are only approximate. In the papers [14,15,57] different correction terms are added to the expressions, which modify the numbers slightly. However, as the derived numbers of Table V in all cases have fairly large uncertainties we have ignored the correction terms. For the systems with AOT we have used $R_0\approx100$ Å [14]. Measurements in systems with nonionic surfactants of the type $C_{10}E_5$ are performed very close to the emulsification boundary. For this reason we have taken $R/R_0=1$ for these measurements.

It should be noted that more values for κ and $\bar{\kappa}$ are available in the literature. These values can of course also be used for deriving the parameters describing the polydispersity and shape fluctuations. But, as mentioned in the Introduction, the parameters vary a lot depending on the experimental method used. In order to keep things relatively simple we decided only to include the values determined from scattering measurements in Table V.

The table demonstrates the inverse dependence between the size of the bending elastic constants κ and $\bar{\kappa}$ and the nonsphericity of the microemulsion droplets. The softer the film the higher the amplitude $\langle|u_{20}|^2\rangle$ and the higher the average axis ratio of the droplet. The relatively small axis ratios determined both from the measurements of Farago *et al.* [14] and by us for AOT microemulsions lead to relatively large numbers for the bending elastic constants, κ and $\bar{\kappa}$. In contrast, the relatively small bending elastic constants κ and $\bar{\kappa}$ determined by Hellweg and Langevin [15,57] for $C_{10}E_5$ microemulsions lead to droplets that, on average, have larger axis ratios.

The numbers determined from our measurements agree quite well with the numbers determined by Farago and coworkers in [14] for the same system as ours but using a different experimental technique. The studies by Hellweg and Langevin [15,57] indicate that the surfactant films in $C_{10}E_5$ microemulsions are much softer than the films formed in AOT microemulsions.

VII. SUMMARY AND CONCLUSION

We have performed measurements of the conductivity as a function of temperature for four symmetric microemulsions made out of AOT/H_2O/*h*-decane, AOT/D_2O/*h*-decane, AOT/D_2O/*d*-decane, and AOT/D_2O/*h*-iso-octane. The mea-

surements show that substituting iso-octane with decane lowers the so-called aggregation temperature by approximately 9 °C. Substituting D_2O with H_2O in the AOT/water/*h*-decane system lowers the aggregation temperature by approximately 8 °C. Changing from *h*-decane to *d*-decane increases the aggregation temperature by only 1 °C.

From SANS measurements on microemulsions with a droplet volume fraction of 5% we have shown that, in approximately the same temperature interval where the conductivity jumps occur in the symmetric microemulsions, aggregation phenomena start to occur in the asymmetric microemulsions. A series of contrast variation measurements have been performed for microemulsions of AOT/D_2O/decane and AOT/D_2O/iso-octane with droplet volume fractions of 5.1% and 5.0%, respectively. The contrast variation is performed by varying the fraction of deuterated alkane. In order to avoid aggregation of the droplets, the measurements were performed at 10 °C and 20 °C, respectively.

The scattering data at zero angle were determined for both systems and analyzed on an absolute scale using a model for polydisperse droplets interacting as hard spheres. The scattering data in the full q range were also analyzed on an absolute scale using a model for polydisperse ellipsoidal droplets that interact as polydisperse hard spheres. The model is fitted simultaneously to all contrasts within each series of measurements, taking the different contrast situations into account.

The polydispersity indices σ/R_{av} determined from the $I(0)$ data are much smaller than the σ/R_{av}'s determined from the scattering data in the full q range. The polydispersity index determined from the $I(0)$ data is very dependent on the absolute value of the few data points measured very close to the match point where the background to noise ratio is large. The analysis of the scattering data in the full q range is based on many more data points and therefore on a much larger amount of information. Therefore the results obtained from the analysis of the full q range are much more reliable.

In both systems, similar water-to-AOT ratios lead to similar average sizes, polydispersities, and size of shape fluctuations. The parameters describing the polydispersities and shape fluctuations are in good agreement with parameters determined earlier [14] for a similar system using a combination of SANS and NSE.

ACKNOWLEDGMENTS

The authors wish to thank Thomas Zemb and Peter Schurtenberger for inspiring discussions.

[1] R. Strey, Colloid Polym. Sci. **272**, 1005 (1994).
[2] M. Gradzielski, D. Langevin, and B. Farago, Phys. Rev. E **53**, 3900 (1996).
[3] T. Sottmann, R. Strey, and S.-H. Chen, J. Chem. Phys. **105**, 6483 (1997).
[4] M. A. Hillmeyer, W. W. Maurer, T. P. Lodge, F. S. Bates, and K. Almdal, J. Phys. Chem. B **23**, 4814 (1999).
[5] M. Kahlweit, R. Strey, R. Schvmacher, and D. Haase, Langmuir **5**, 305 (1989).
[6] H. Kunieda and K. Shinoda, J. Colloid Interface Sci. **75**, 601 (1980).
[7] H. Kunieda and K. Shinoda, J. Colloid Interface Sci. **70**, 577 (1979).
[8] W. Sager, Langmuir **14**, 6385 (1998).
[9] J. Rička, M. Borkovec, and U. Hofmeier, J. Chem. Phys. **94**, 8503 (1991).
[10] S. Christ and P. Schurtenberger, J. Phys. Chem. **98**, 12 708 (1994).
[11] J. C. Eriksson and S. Ljunggren, Prog. Colloid Polym. Sci. **81**, 41 (1990).
[12] J. C. Eriksson and S. Ljunggren, Langmuir **11**, 1145 (1995).
[13] C. Robertus, W. H. Philipse, J. G. H. Joosten, and Y. K. Levine, J. Chem. Phys. **90**, 4482 (1989).
[14] B. Farago, D. Richter, J. S. Huang, S. A. Safran, and S. T. Milner, Phys. Rev. Lett. **65**, 3348 (1990).
[15] T. Hellweg and D. Langevin, Physica A **264**, 370 (1999).
[16] F. Sicoli, D. Langevin, and L. T. Lee, J. Chem. Phys. **99**, 4759 (1993).
[17] J. Eastoe, D. Sharpe, R. K. Heenan, and S. Egelhaaf, J. Phys. Chem. B **101**, 944 (1997).
[18] M. Almgren, R. Johannsson, and J. C. Erikson, J. Phys. Chem. **97**, 8590 (1993).
[19] M. Gradzielski, D. Langevin, T. Sottmann, and R. Strey, J. Chem. Phys. **106**, 8232 (1997).
[20] M. Borkovec, Adv. Colloid Interface Sci. **37**, 195 (1992).
[21] S. A. Safran, Phys. Rev. A **43**, 2903 (1991).
[22] M. Gradzielski, Curr. Opin. Colloid Interface Sci. **3**, 478 (1999).
[23] E. Caponetti, M. A. Floriano, E. Di Dio, and R. Triolo, J. Appl. Crystallogr. **26**, 612 (1993).
[24] K. Mortensen, Nukleonika **39**, 169 (1994).
[25] J. S. Pedersen, in *Modern Aspects of Small Angle Scattering*, edited by H. Brumberger (Klüwer Academic Publishers, Dordrecht, 1995).
[26] A wavelength spread of 24% (FWHM) corresponds to a σ/R of around 10% and, as the widths of independent Gaussians add up in quadrature, the contribution to the scattering pattern from the wavelength spread is still small compared to the contribution from the size polydispersity of the microemulsion droplets, which normally has $\sigma/R \approx 15-20$ %.
[27] B. Jacrot, Rep. Prog. Phys. **39**, 911 (1976).
[28] J. S. Pedersen, D. Posselt, and K. Mortensen, J. Appl. Crystallogr. **23**, 321 (1990).
[29] L. Arleth and J. S. Pedersen, J. Appl. Crystallogr. **33**, 650 (2000).
[30] C. Robertus, J. G. H. Joosten, and Y. K. Levine, Phys. Rev. A **42**, 4820 (1990).
[31] G. J. M. Koper, W. F. C. Sager, J. Smeets, and D. Bedeaux, J. Phys. Chem. **99**, 13 291 (1995).
[32] M. Kotlarchyk, S.-H. Chen, J. S. Huang, and M. W. Kim, Phys. Rev. A **29**, 2054 (1984).
[33] J. S. Huang, S. A. Safran, M. W. Kim, G. S. Grest, M. Kotlarchyk, and M. Quirke, Phys. Rev. Lett. **53**, 592 (1984).

[34] A. Jada, J. Lang, and R. Zana, J. Chem. Phys. **93**, 10 (1989).
[35] W. F. C. Sager, W. Sun, and H.-F. Eicke, Prog. Colloid Polym. Sci. **89**, 284 (1992).
[36] P. Alexandridis, J. F. Holzwarth, and T. A. Hatton, J. Phys. Chem. **99**, 8222 (1995).
[37] O. Glatter, J. Appl. Crystallogr. **10**, 415 (1977).
[38] J. S. Pedersen, Adv. Colloid Interface Sci. **70**, 171 (1997).
[39] P. van Beurten and A. Vrij, J. Chem. Phys. **74**, 2744 (1981).
[40] Lord Rayleigh; Proc. R. Soc. London, Ser. A **84**, 25 (1911).
[41] A. Guinier, Ann. Phys. (Paris) **12**, 161 (1939).
[42] Expressions for the surface areas of prolate and oblate spheroids can be found, for example, in *Handbook of Mathematical Sciences*, edited by W. H. Beyer (CRC Press, Boca Raton, 1978).
[43] A. Vrij, J. Chem. Phys. **69**, 1742 (1978).
[44] A. Vrij, J. Chem. Phys. **71**, 3267 (1979).
[45] J. S. Pedersen, Phys. Rev. B **47**, 657 (1993).
[46] Y. D. Yan and J. H. R. Clarke, J. Chem. Phys. **93**, 4501 (1990).
[47] W. H. Press, S. A. Teukolsky, W. T. Vetterling, and B. P. Flannery, *Numerical Recipes in Fortran* (Cambridge University Press, Cambridge, 1992).
[48] P. R. Bevington, *Data Reduction and Error Analysis for the Physical Sciences* (McGraw-Hill, New York, 1969).
[49] Information from the manufacturers.
[50] J. S. Pedersen, Report No. Risø-R-1166(EN), Risø National Laboratory, Roskilde, Denmark, 1999, p. 51 (unpublished), p. 51. Available on request from: Riso National Laboratory Information Service Department, P.O. Box 49, DK-4000 Roskilde, Denmark.
[51] D. Svergun, Proc. Natl. Acad. Sci. U.S.A. **95**, 2267 (1998).
[52] A. N. North, J. C. Dore, J. A. Mcdonald, B. H. Robinson, R. H. Heenan, and A. M. Howe, Colloids Surface **19**, 21 (1986).
[53] D. Svergun, P. V. Konarev, V. V. Volkov, M. H. J. Koch, J. Smeets, and W. F. C. Sager (unpublished); D. I. Svergun, P. V. Konarev, V. V. Volkov, M. H. J. Koch, W. F. C. Sager, J. Smeets, and J. Blokhuis, J. Chem. Phys. **113**, 1651 (2000).
[54] D. Frenkel and B. M. Mulder, Mol. Phys. **55**, 1171 (1985).
[55] S. T. Milner and S. A. Safran, Phys. Rev. A **36**, 4371 (1987).
[56] S. A. Safran, J. Chem. Phys. **78**, 2073 (1983).
[57] T. Hellweg and D. Langevin, Phys. Rev. E **57**, 6825 (1998).